Chemical Geology 400 (2015) 44–55

Contents lists available at ScienceDirect

Chemical Geology

journal homepage: www.elsevier.com/locate/chemgeo

Pyrite formation and mineral transformation pathways upon sulfidation of ferric hydroxides depend on mineral type and sulfide concentration

Stefan Peiffer [a,*], Thilo Behrends [b], Katrin Hellige [a,1], Philip Larese-Casanova [c], Moli Wan [a,1], Kilian Pollok [d,e]

[a] Department of Hydrology, Universität Bayreuth, Universitätsstraße 30, D-95445 Bayreuth, Germany
[b] Department of Earth Sciences, Geochemistry, Utrecht University, P.O. Box 80021, 3508 TA Utrecht, The Netherlands
[c] Department of Civil and Environmental Engineering, Northeastern University, 469 Snell Engineering, 360 Huntington Ave, Boston, MA 02115, USA
[d] Bayerisches Geoinstitut, Universität Bayreuth, Universitätsstraße 30, D-95445 Bayreuth, Germany
[e] Institute of Geosciences, Mineralogy, Friedrich-Schiller-Universität Jena, Carl-Zeiss-Promenade 10, D-07745 Jena, Germany

ARTICLE INFO

Article history:
Received 23 April 2014
Received in revised form 29 January 2015
Accepted 31 January 2015
Available online 9 February 2015

Editor: Michael E. Böttcher

Keywords:
Ferric hydroxides
Dissolved sulfide
Ferrous iron
Pyrite formation
Electron transfer
Bulk mineral electrons

ABSTRACT

The reaction of ferric (hydr)oxides with dissolved sulfide does not lead to the instantaneous production of thermodynamically stable products but can induce a variety of mineral transformations including the formation of metastable intermediates. The importance of the various transformation pathways depends, among other factors, on the characteristics of the ferric (hydr)oxides but a mechanistic model which relates the mineralogy of the ferric (hydr)oxides to the type of reaction products and their evolution over time is still missing. Here, we investigate the kinetics of the reaction between dissolved sulfide (6.7–7.5 mmol L^{-1}) with ferrihydrite (Fh, 12 mmol L^{-1}), lepidocrocite (Lp, 26.6 mmol L^{-1}), and goethite (Gt, 22 mmol L^{-1}) in batch experiments at pH 7 and room temperature. The time evolution of solution and solid phase composition was monitored over 2 weeks while TEM, and Mössbauer spectroscopy were used to characterize the transformations of the solid phases.

Dissolved sulfide was consumed within 2 (Fh, Lp) to 8 h (Gt) with methanol extractable sulfur and HCl extractable Fe(II) ($Fe(II)_{HCl}$) being the main products after this time. The mass balances of Fe and S indicated that a large fraction of the $Fe(II)_{HCl}$ in the reactions with Fh (46% of $Fe(II)_{HCl}$) and Lp (36% of $Fe(II)_{HCl}$) was solid-phase bound but not associated with sulfur. This excess Fe(II) exceeded the adsorption capacity of the solids and remained associated with the oxides. Over the time scale of days, the concentrations of MES and $Fe(II)_{HCl}$ decreased and this process was accompanied by the formation of secondary iron oxides and pyrite in all experiments. The pyrite yield after two weeks showed the same trend as the amounts of intermediately produced excess Fe(II): Fh (84% of initial S(−II)) > Lp (50%) > Gt (13%). Besides the formation of pyrite, Fh transformed completely into thermodynamically more stable iron oxides such as hematite or magnetite. In contrast, formation of other iron oxides was only minor when Lp or Gt reacted with sulfide.

We propose that the extent of pyrite and secondary iron mineral precipitation is controlled by the ratio between the competing formation rates of excess Fe(II) and surface bound FeS (FeS_s) in the early stage of the reaction. Formation of excess Fe(II) is a prerequisite for rapid pyrite formation and induces secondary formation of iron oxides. The competition between excess Fe(II) and FeS_s formation, in turn, is ruled by two factors: 1) the ratio between added sulfide and available surface area, and 2) the capability of the iron(hydr)oxide to conduct electrons from surface bound Fe(II) to bulk Fe(III) and to accommodate structural Fe(II). This capability is largest for Fh and explains the most pronounced excess Fe(II) production and, by this, the greatest pyrite yield in experiments with Fh. During the reaction with Gt, in contrast, formation of FeS_s outcompetes the accumulation of excess Fe(II) and consequently the precipitation of pyrite is only minor.

This conceptual model constrains conditions at which relatively fast pyrite formation within the time scale of days or weeks might be relevant in natural environments. Suitable conditions are expected in environments with low sulfide levels in which formation of reactive iron (hydr)oxides is stimulated by redox oscillations (e.g., wetlands, riparian soils, tidal flats).

1. Introduction

Reduction of ferric (hydr)oxides is a prominent pathway contributing to electron fluxes in subsurface environments (Raiswell and

* Corresponding author. Tel.: +49 921 552253; fax: +49 921 552366.
E-mail address: s.peiffer@uni-bayreuth.de (S. Peiffer).
[1] Tel.: +49 921 552251; fax: +49 921 552366.

http://dx.doi.org/10.1016/j.chemgeo.2015.01.023
0009-2541/

Canfield, 2011) and is directly connected to the bioavailability and mobility of nutrients (Einsele, 1936) and contaminants (Haderlein and Pecher, 1998). Reductive dissolution occurs either enzymatically (e.g., /INS; Thamdrup, 2000) or chemically (Cornell and Schwertmann, 2003) with dissolved sulfide being a powerful and ubiquitous reductant in anoxic environments (e.g., Canfield et al, 1992). Ferric (hydr)oxides display a wide spectrum of reactivity (Postma, 1993) as being controlled by surface area (Roden, 2003) but also by thermodynamic properties such as E_h (Fischer, 1987) or solubility product (Bonneville et al, 2009). Interaction with sulfide is regarded to be a surface controlled process (Dos Santos Afonso and Stumm, 1992; Peiffer et al., 1992). Under acidic conditions Fe(II) becomes completely dissolved (Peiffer and Gade, 2007) whereas solid FeS is a common initial product at circumneutral pH (Rickard, 1974; Pyzik and Sommer, 1981).

It has been early recognized that sulfidation of ferric (hydr)oxides also triggers the formation of pyrite (Rickard, 1975). The accepted model for pyrite formation is the reaction between an aqueous FeS species and dissolved polysulfides, which requires solid FeS as a precursor species (cf. review in Rickard, 2012 and references therein), irrespective of the origin of the reactants. In a recent study, it was demonstrated that sulfidation of lepidocrocite at millimolar S(−II) concentration and at pH 7 is a highly dynamic process (Hellige et al, 2012). High resolution transmission electron microscopy (HRTEM) revealed that lepidocrocite crystals were covered with FeS after 2 h when dissolved S(−II) was completely consumed. FeS started to disappear after 72 h along with the formation of amorphous Fe and S phases. Nanopyrite particles formed after only one week. Cryogenic X-ray photoelectron spectroscopy measurements demonstrate that a substantial fraction (>50%) of the S species consisted of surface-bound polysulfides (Wan et al., 2014) with only small amounts (<1%) of the initial sulfide being recovered as aqueous polysulfides.

Poulton et al. (2004) investigated the reaction of various ferric (hydr)oxides with dissolved sulfide at pH 7.5 and observed the accumulation of acid extractable Fe(II) which is neither Fe(II) extractable as acid volatile sulfur (AVS) nor is it exchangeable with other cations. They considered this fraction to be associated with the surface, but the amount of Fe(II) in this pool exceeded in lepidocrocite the number of sites at the oxide surface by a factor of 10. The nature of this Fe(II) containing phase remained unclear. Similarly, a significant fraction of solid-phase Fe(II) in excess to surface Fe(II) associated with sulfur species was observed during sulfidation of lepidocrocite (Hellige et al, 2012). The excess Fe(II) was interpreted as uptake of electrons into the bulk mineral (Gorski and Scherer, 2012). The amount of produced pyrite was higher in experiments in which high concentrations of excess Fe(II) were intermediately formed. It was therefore proposed that the pool of excess Fe(II) triggered the sequence of mineral transformations and promoted the formation of pyrite.

The relative importance of excess Fe(II) formation during the reaction may also depend on the type of ferric iron (hydr)oxide. Poulton et al (2004) observed a range in reactivity towards sulfide covering two orders of magnitude when normalized to surface area. According to our proposed model, channeling of electrons into the bulk structure can therefore be expected to be less significant at low reactivity, i.e. higher crystallinity.

We therefore hypothesize that the extent of excess Fe(II) production and hence the extent of pyrite formation upon sulfidation is different for various ferric (hydr)oxides and depends on their electron transfer properties, but also on their ability to accommodate Fe(II) within the structure. Adsorption of Mössbauer-insensitive ^{56}Fe(II) to various ferric (hydr)oxides revealed dramatic variations in magnetic response of ferrihydrite (Williams and Scherer, 2004), hematite (Larese-Casanova and Scherer, 2007), magnetite (Gorski and Scherer, 2009) and goethite (Gorski and Scherer, 2012) that is being attributed to a varying degree of electron delocalization in the bulk minerals (Gorski and Scherer, 2012). As a consequence, type and concentrations of secondary Fe minerals such as pyrite forming upon the reaction with S(−II) are expected to differ between different ferric iron (hydr)oxides in relation to the relative production of excess Fe(II).

Here, we compare the reductive dissolution of lepidocrocite with those of ferrihydrite and goethite, representing a less stable and a more stable iron oxide phase, respectively. We conducted batch experiments with the same set-up and analytical methods as described in Hellige et al. (2012) with a focus on the reactivity of these hydr(oxides) in sulfide-rich systems at pH 7 in regard to the reaction rates, intermediate phases, and final products.

2. Materials and methods

2.1. Ferric (hydr)oxides

Synthetic 6-line ferrihydrite was prepared after Schwertmann and Cornell (2000). Under rapid stirring, 20 g of $Fe(NO_3)_3 \cdot 9H_2O$ was added to 2 L 75 °C hot distilled water. After 12 min of stirring, the solution was cooled and dialyzed for three days. The final product was freeze dried.

Synthetic lepidocrocite and goethite were purchased from Lanxess (Leverkusen, Germany). The trade names are Bayferrox 920 Z for goethite and Bayferrox 943 for lepidocrocite. To remove sulfate from the iron oxide surface (which commercial ferric (hydr)oxides typically contain), 1 mol L^{-1} of each hydroxide was suspended in 0.01 mol L^{-1} $NaNO_3$ and the pH was adjusted to 10 with NaOH. After 4 days of shaking the suspension was washed and freeze-dried.

The ferric (hydr)oxides were characterized using X-ray diffractometry (XRD), scanning electron microscopy (SEM), and transmission electron microscopy (TEM). Lepidocrocite contained 5–10 wt.% goethite and had a particle size of 0.2–0.4 μm as determined by SEM. Goethite had a particle size of 0.2–0.9 μm. Ferrihydrite particles were <10 nm as revealed by TEM (cf. Fig. 6). Surface area was measured by multipoint BET-N_2 (Brunauer, Emmett and Teller) method (Gemini 2375 Surface Area Analyzer). Surface areas were determined to be 140 m^2 g^{-1} for ferrihydrite, 17.34 m^2 g^{-1} for lepidocrocite and 9.12 m^2 g^{-1} for goethite.

2.2. Experimental set-up

Kinetic batch experiments were conducted in an anoxic glove box at pH 7 at a constant ionic strength of I = 0.1 mol L^{-1} NaCl and at room temperature. In this publication data are presented from those three experiments only where we have a complete data set in regard to wet chemical analysis, TEM and Mössbauer spectroscopy. Additional results from lepidocrocite experiments have been published in Hellige et al (2012). Ferric (hydr)oxide concentrations in these three experiments ranged between 12 and 26.6 mmol L^{-1} and the initial dissolved sulfide concentration between 6.7 and 7.5 mmol L^{-1} (cf. Table 1). Initial sulfide concentrations were in large excess relative to initial surface site concentrations of the three mineral phases (Table 1). All reactions were conducted in a 500-mL glass vessel with ports for sampling, addition of reactants and for a pH electrode. The solution was stirred with a Teflon-coated stirring bar at constant rate. With an automatic pH-stat device the pH value was kept constant by adding HCl (0.5 mol L^{-1}) in the glove box. The reaction suspension was prepared by mixing 50 mL of 0.1 mol L^{-1} NaCl solution containing approx. 1 g ferric (hydr)oxide with 450 ml of 0.1 mol L^{-1} NaCl to which appropriate amounts of NaHS (as a 1:1. mixture between $Na_2S \cdot 9H_2O$ (0.5 mol L^{-1}) and HCl (0.5 mol L^{-1})) were added. In order to convert the mass of the ferric (hydr)oxides into molar concentrations, the molar mass of ferrihydrite was determined to be 92.3 g/mol after dissolution in 6 N HCl and determination of Fe. Molar masses of 89 g/mol were used for lepidocrocite and goethite. The sulfide concentration was determined before each run.

During the reaction, aliquots were taken to monitor the time evolution of dissolved Fe(II) and S(−II), Fe(II) extractable with 0.5 N HCl,

Table 1
Initial experimental conditions for experimental runs where both TEM and Mössbauer spectroscopy was performed. All runs were conducted at pH 7.

Mineral	Fe concentration mmol L^{-1}	Surface area concentration m^2 L^{-1}	Concentration of surface sites[a] mmol L^{-1}	Initial sulfide concentration mmol L^{-1}	S(−II): surface site ratio [−]
Ferrihydrite	12	155	0.98	7.5	7.7
Lepidocrocite	26.6	41.1	0.26	7.2	27.8
Goethite	22	17.9	0.11	6.7	57.6

[a] Concentration of surface sites was calculated based on a value of $6.3 \cdot 10^{-6}$ mol m^{-2} for all minerals (Peiffer and Gade, 2007).

methanol extractable sulfur, and total iron. Furthermore, solids were retrieved after 1–2 h, 24 h, 1 week and 2 weeks and analyzed by Mössbauer spectroscopy and TEM. All solutions were prepared with distilled water and purged with N_2 prior to use to remove dissolved oxygen from solutions. All reagents were of analytical grade.

2.3. Sampling and analysis

2.3.1. Iron species

Dissolved Fe(II) ($Fe(II)_{diss}$) was determined after filtration (0.45 μm) using the phenanthroline method (Tamura et al, 1974). Total extractable iron was determined in the suspension prior to the addition of sulfide after dissolution in 6 N HCl and heating at 60 °C for 3 days. HCl extractable Fe(II) ($Fe(II)_{HCl}$), which comprises both dissolved and solid phase-bound Fe(II), was extracted with 0.5 N HCl for 1 h and briefly (2–3 min) purged with N_2, filtered and the Fe(II) was determined in the filtrate as described above. The occurrence of surface bound iron sulfide (FeS_s) and iron associated with polysulfides ($FeS_{n,s}$) in the samples may lead to an overestimation of HCl extractable Fe(II) through reaction of the liberated H_2S with ferric iron in the acidic extraction solution. In order to test the effect of this reaction on the yield of Fe(II), we have added aliquots of a FeS suspension to a suspension of a predefined amount of the respective ferric hydroxide to obtain a final concentration of 2, 4, 8 and 13.5 mmol L^{-1} FeS and 2 g L^{-1} of ferric hydroxide and extracted Fe(II) with 0.5 N HCl at different time steps. FeS was prepared by precipitation from Na_2S ($c = 0.4$ mol L^{-1}) and $FeCl_2 \cdot 4H_2O$ ($c = 0.4$ mol L^{-1}) in a glove box to obtain a stock solution of 0.2 mmol L^{-1} FeS. Dissolved sulfide and Fe(II)aq in the stock solution were 68 μmol L^{-1} and 16 μmol L^{-1} respectively. Recovery rates after 1 h ranged between 196% and 232% for the four FeS concentrations in case of ferrihydrite. In case of lepidocrocite and goethite, only 13.5 mmol L^{-1} FeS were tested to yield a recovery of 101% and 95%, respectively. Hence, measured $Fe(II)_{HCl}$ concentrations were overestimated by about a factor of two when FeS and ferrihydrite were simultaneously extracted. Therefore, in experiments with ferrihydrite a correction factor of two was applied for calculating the amount of excess Fe(II) (Eq. (1)). In the experiments with goethite and lepidocrocite, the increase of $Fe(II)_{HCl}$ due to the reduction of Fe(III) during HCl extraction seemed to be within the range of uncertainty.

2.3.2. Sulfur species

Dissolved sulfide ($S(-II)_{diss}$) was determined photometrically by the methylene blue method (Fonselius et al, 1999) after filtration. Methanol extractable sulfur (MES) was measured by high performance liquid chromatography (HPLC, Beckman) combined with UV detection (Detector 168, Beckman) after extraction of 300 μL of unfiltered sample suspended in 1200 μL methanol (modified after Ferdelman et al., 1991). Wan et al. (2014) demonstrated that MES comprises not only elemental S_8 sulfur but also zero-valent sulfur from polysulfides associated with the ferric (hydr)oxides surface, probably as Fe(II)-polysulfide associations. After 1 h equilibration time, the suspension was filtered (0.2 μm) and the filtrate was stored at −20 °C until analysis. The precision of this method was estimated from measurements of MES after 10 min of reaction of dissolved sulfide with lepidocrocite. The data were taken from five independent experiments documented in Hellige (2011). Since initial concentrations of both dissolved sulfide and lepidocrocite where different in each experiment, it was not possible to calculate the mean value and the standard deviation of the MES measurement. Hence, the relative error was calculated from the amount of MES recovered per mol lepidocrocite and was 13%.

2.3.3. Mössbauer spectroscopy

30 mL of the suspension was centrifuged outside the glove box using closed centrifuge tubes. After centrifugation, the supernatant was decanted inside the glove box and the solid phase was dried under a nitrogen stream for 1 min. After drying, the solid phase was put on a membrane filter (13 mm diameter and 0.45 μm) and was sealed between two layers of Kapton tape (polyimide tape with very low oxygen permeability). The samples were placed in a sealed crimp vial and stored at 4 °C until measurement. Mössbauer spectra were collected with a WissEl Mössbauer gamma-ray spectrometer and a Janis closed-cycle helium gas cryostat at 4.2 K. A Co-57 gamma-ray source was used with a constant acceleration drive system operated in transmission mode. Spectra were calibrated against a spectrum of alpha-Fe(0) foil at room temperature. Data acquisition times were usually about 12–20 h per spectrum. Spectral fitting was performed using Recoil® software (University of Ottawa, Canada) and Voigt-based spectral lines. Model parameters from the various specimens are listed in Table 2. The concentrations of iron mineral phases were calculated by multiplying total Fe concentration by their fitted spectral area, which represents the percentage of the individual mineral phases. The detection limit of Mössbauer spectroscopy is ~2% of total Fe.

2.3.4. Transmission electron microscopy

Aliquots of the reacting suspension (after 2 h and 2 weeks) were analyzed by a Philips CM 20-FEG TEM (Bayerisches Geoinstitut, University of Bayreuth), operating at 200 kV. In order to minimize oxidation in air during sample preparation the aliquots collected from the experimental suspension were stored in gas-tight vials until TEM analysis. Immediately before transfer of the sample into the TEM, a drop of the suspension was then taken with a syringe and put onto a Lacey carbon-coated copper grid. The grid was immediately transferred to the TEM holder and inserted into the high vacuum of the TEM. The short exposure of the sample to air was limited to 1–2 min at maximum with this procedure. The chemical composition and the distribution of elements were determined by energy dispersive X-ray (EDX) spectroscopy (Thermo Noran Ge detector).

3. Results

3.1. Chemical speciation

In the presence of ferrihydrite and lepidocrocite, dissolved sulfide was consumed within 30 min. In contrast, the reaction was slower when goethite was added and more than 5 h were required to quantitatively remove the added dissolved sulfide (Fig. 1). The consumption of $S(-II)_{aq}$ was accompanied by the production of Fe(II) and MES (Fig. 1). In all cases, the concentration of dissolved Fe(II) represented only a minor fraction of $Fe(II)_{HCl}$ with a maximum concentration of 0.3 mmol L^{-1} (data not shown). In experiments with ferrihydrite and lepidocrocite, $Fe(II)_{HCl}$ concentrations reached almost instantaneously a level which remained practically constant during the first hour of

Table 2
Concentrations of products during the reaction of H_2S with the three ferric (hydr)oxides after constant values were reached. Values for ferrihydrite and lepidocrocite correspond to t = 2 h, while those for goethite to t = 8 h.

Mineral	$H_2S_{initial}$ (mmol L^{-1})	S^0 (mmol L^{-1})	$Fe(II)_{HCl}$ (mmol L^{-1})	Excess Fe(II) (mmol L^{-1})	Fraction of excess Fe(II) (%)	Protons consumed (mmol L^{-1})
Ferrihydrite	7.5	5.1	9.0	4.2	46	1.2
Lepidocrocite	7.2	3.7	5.5	2.0	36	2.4
Goethite	6.7	1.5	4.5	−0.7	0	2.8

reaction (Fig. 1). Production of $Fe(II)_{HCl}$ also followed $S(-II)_{aq}$ consumption in the experiments with goethite and, consequently, was slower compared to the reaction with ferrihydrite and lepidocrocite. It required about 5 h, before the increase of $Fe(II)_{HCl}$ ceased.

The stoichiometric ratio between the concentration of Fe(II) produced until a constant $Fe(II)_{HCl}$ level had established and the $S(-II)_{aq}$ concentration consumed varied between the different starting materials (Table 3) ranging from 1.20 for ferrihydrite, 0.76 for lepidocrocite to 0.67 for goethite. Similar experiments performed with various initial concentrations of lepidocrocite demonstrated that ratios >0.8 coincide with a significant fraction of excess Fe(II) not bound in the form of Fe(II) associated with sulfur (cf. Table 3 in Hellige et al, 2012). Observations made by Wan et al. (2014) imply that Fe(II) associated with surface polysulfide ($FeS_{n,s}$) can be also extracted with HCl. Hence $Fe(II)_{HCl}$ comprises FeS_s, $Fe(II)_{excess}$, and $FeS_{n,s}$. The results from that study further imply that the concentration of these surface Fe(II) sulfur species (FeS_s and $FeS_{n,s}$) can be estimated by the concentration difference between initially added sulfide and MES. We therefore calculated the amount of excess Fe(II) based on the S mass balance as

$$\begin{aligned} c(\text{excess}-\text{Fe(II)}) &= c(\text{Fe(II)}_{HCl}) - F \cdot \left[c(FeS_s) + c\left(FeS_{n,s}\right)\right] \\ &= \text{Fe(II)}_{HCl,const} - F \cdot \left[c(S(-II)_{initial}) - c(MES_{const})\right], \end{aligned} \quad (1)$$

where $Fe(II)_{HCl,const}$ and MES_{const} are concentrations of $Fe(II)_{HCl}$ and MES after a constant concentration level was obtained, i.e. 2 h in case of ferrihydrite and lepidocrocite and 8 h in case of goethite. F is a correction factor that accounts for the generation of Fe(II) through reaction between Fe(III) and H_2S liberated from FeS_n species during the extraction. Based on the recovery tests of $Fe(II)_{HCl}$ in the presence of FeS_n species, F was set to be 2 for ferrihydrite, and 1 for lepidocrocite and goethite, respectively.

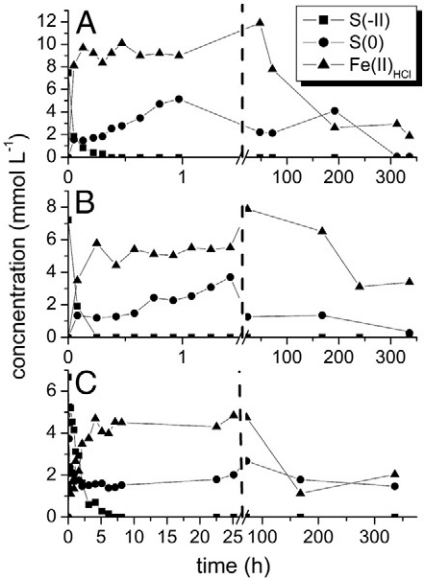

Fig. 1. Time evolution of sulfur and iron species during the reaction between dissolved sulfide and ferrihydrite (A), lepidocrocite (B), and goethite (C). Note the different time scale for goethite.

The largest fraction of Fe(II) in excess of FeS_s and $FeS_{n,s}$ was found for ferrihydrite (~46% of HCl extractable Fe(II)). It was smaller for lepidocrocite (36%) and even negative for goethite (Table 3). The negative value probably reflects the uncertainty inherent to the analytical methods so that the fraction of excess Fe(II) is assumed to be zero in case of goethite.

In the presence of ferrihydrite, the concentration of $Fe(II)_{HCl}$ achieved a maximum of almost 12 mmol L^{-1} at 48 h. Even if one accounts for an overestimation of extractable Fe(II) due to interference with AVS during acidic extraction, a significant fraction of the initial amount of Fe(III) in ferrihydrite was reduced (Fig. 1A). After 48 h, however, $Fe(II)_{HCl}$ and MES started to decrease for all three minerals. The decrease was more pronounced for $Fe(II)_{HCl}$ and most prominent in experiments with ferrihydrite (Fig. 1A).

Visually, all ferric suspensions turned black during the reaction with dissolved sulfide indicating formation of a solid FeS phase. After 2 weeks the black coloration of the suspensions disappeared for goethite and lepidocrocite while the ferrihydrite suspension remained black.

When constant concentration levels of MES and $Fe(II)_{HCL}$ were established, H^+ consumption was comparable for lepidocrocite and goethite with 2.4 mmol L^{-1} after 2 h and 2.8 mmol L^{-1} after 8 h, respectively (Fig. 2). Additional 0.8 mmol L^{-1} (lepidocrocite) and 0.4 mmol L^{-1} (goethite) of alkalinity were generated in the following 2 weeks. In the reaction with ferrihydrite, the amount of consumed H^+ was distinctly lower with only 1.2 mmol L^{-1} H^+ after 2 h and additionally 0.4 mmol L^{-1} H^+ in the following 2 weeks. A drop in pH which could not be balanced by the pH-stat device (addition of HCl) occurred after 250 h in the experiment with ferrihydrite and lepidocrocite.

The three ferric (hydr)oxides showed the same chemical reaction pattern but the velocity of dissolved sulfide consumption was different. The reactivity was very high for lepidocrocite and ferrihydrite with the initial rate constant k_{obs} being in the same order of magnitude (~$5 \cdot 10^{-3}$ L m^{-2} min^{-1}). It was significantly slower for goethite ($5 \cdot 10^{-4}$ L m^{-2} min^{-1}, cf. also Fig. 1). Initial rate constants k_{obs} were determined as pseudo first-order rate constant obtained from the concentration change of $c(S(-II)_{aq})$ with time divided by the surface area concentration of the ferric (hydr)oxides. Values for ferrihydrite and lepidocrocite bear some uncertainty due to the poor time resolution.

3.2. Spectroscopic and microscopic results

3.2.1. Mössbauer spectroscopy

Mössbauer spectra revealed a dynamic transformation process with distinct differences between the three oxyhydroxides. The dominant signal in spectra from solids collected in experiments with lepidocrocite and goethite (Figs. 3 and 4) could be clearly attributed to the starting minerals. Six-line signals (sextets) with narrow line-widths were identified as lepidocrocite and goethite, respectively, based on model parameters that were consistent with an oxidation state of Fe(III) in a high-spin octahedral configuration similar to that in synthetic minerals with Fe(III) in its antiferromagnetic state.

Table 3
Model parameters used for evaluation of 4.2 K Mössbauer spectra and abundances of the minerals identified.

Sample time	Fe(III) sextet								FeS_2		
	I[a] mm s^{-1}	χ^{2}[b]	<CS>[c] mm s^{-1}	<QS>[d] mm s^{-1}	<H>[e] T	# of comp.[f]	Hp[g] T	Abundance	<CS> mm s^{-1}	<QS> mm s^{-1}	Abundance
Ferrihydrite			*Fe(III) sextet*								
1 h	–	–	–	–	–	–	–	–	–	–	–
1 day	–	–	–	–	–	–	–	–	–	–	–
1 week	0.11	4.0	0.49	−0.11	49.1	2	50.1	70.7	0.41	0.62	29.3
2 weeks	0.11	2.0	0.48	−0.10	48.8	2	49.9	73.6	0.40	0.64	26.4
Lepidocrocite			*Lepidocrocite sextet*								
1 h	0.11	1.4	0.50	0.04	44.8	2	45.4	100	–	–	–
1 day	0.11	2.0	0.50	0.04	43.7	3	45.5	100	–	–	–
1 week	0.11	1.3	0.50	0.04	43.9	3	45.5	98.2	0.42	0.60	1.8
2 weeks	0.11	2.0	0.50	0.03	44.4	2	45.4	93.4	0.40	0.65	6.6
Goethite			*Goethite sextet*								
1 h	0.11	1.6	0.49	−0.23	50.6	1	50.6	100	–	–	–
1 day	0.11	2.9	0.49	−0.23	50.6	1	50.6	100	–	–	–
1 week	0.11	2.3	0.49	−0.23	50.6	1	50.6	91.6	0.40	0.64	8.4
2 weeks	0.11	1.5	0.49	−0.23	50.6	1	50.6	98.0	0.40	0.64	2.0
Mineral standards											
Ferrihydrite, 4.2 K			0.48	−0.02	47.4	2	49.9				
Goethite, 4.2 K			0.48	−0.25	50.6	1	50.6				
Pyrite, 77 K									0.36	0.64	
Pyrite, 4.2 K									0.43	0.66	
Marcasite, 80 K									0.37	0.50	
Magnetite, 4.2 K	^{IV}Fe(III)		0.37	−0.02	50.1						
	^{VI}Fe(III) 1[h]		0.49	0.00	52.2						
	^{VI}Fe(III) 2[h]		0.83	−0.27	49.8						
	^{VI}Fe(II) 1[h]		1.03	−0.41	48.2						
	^{VI}Fe(II) 2[h]		0.96	0.89	35.9						

[a] Lorenztian half-width at half-maximum.
[b] Reduced chi-squared goodness of fit value.
[c] Average center shift.
[d] Average quadrupole splitting.
[e] Average hyperfine magnetic field.
[f] Number of Voigt-based components used to model the hyperfine magnetic field.
[g] Most probable hyperfine magnetic field value.
[h] Numbers refer to sites of the corresponding octahedra.

In contrast to lepidocrocite and goethite, sextets were present after one week within spectra of solids from the original ferrihydrite experimental suspensions (Fig. 5). These sextets demonstrate abundance of iron in the Fe(III) oxidation state but they do not provide clear indication for the presence of ferrihydrite. The broad peaks and the large number of parameters (cf. Table 2) made it impossible to find a unique solution. The sextets represent iron which is magnetically ordered at this temperature and belong to a mixture of various minerals that may represent a combination of goethite, hematite, and magnetite as observed in TEM spectra (cf. below). Unfortunately, we could not collect enough material for the analysis of the first two samples of the ferrihydrite experiments taken after 1 h and 24 h (data not shown).

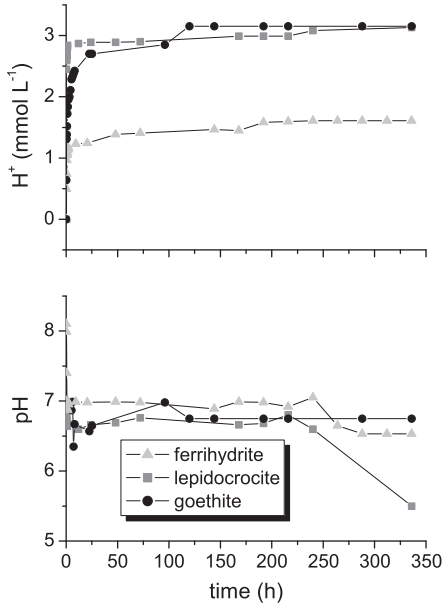

Fig. 2. pH progress (bottom) and H^+ consumption (top) during the reaction between ferrihydrite, lepidocrocite, and goethite with dissolved sulfide.

In spite of the large fraction of excess Fe(II) that was derived from wet chemical analyses in the presence of ferrihydrite and lepidocrocite in the initial phases of the experiment (Eq. (1)), no signals could be retrieved from the Mössbauer spectra that could be attributed to an Fe(II) containing phase.

After one week a second signal emerged in the form of a doublet in the presence of all ferric hydroxides. We exclude the possibility of this signal being an iron (hydr)oxide phase because crystalline iron (hydr) oxides, even paramagnetic ones, do not produce doublet signals at 4.2 K and instead produce sextet signals. However, diamagnetic iron sulfides such as pyrite and marcasite can remain as doublet signals when analysis temperature is 4.2 K (Murad and Cashion, 2004). Pyrite and marcasite share the same unit cell formula (FeS_2) and have low-spin octahedral Fe(II) configurations with paired d-orbital electrons that allow the minerals to remain paramagnetic at 4.2 K.

The abundance of FeS_2 was very high (almost 30%) in ferrihydrite experiments after 1 week and slightly decreased or remained constant after 2 weeks (Table 2, Fig. 5). In the lepidocrocite experiments, the abundance was significantly smaller in the first week (1.8%, Table 2, Fig. 3) compared to ferrihydrite but strongly increased to 6.6% by the

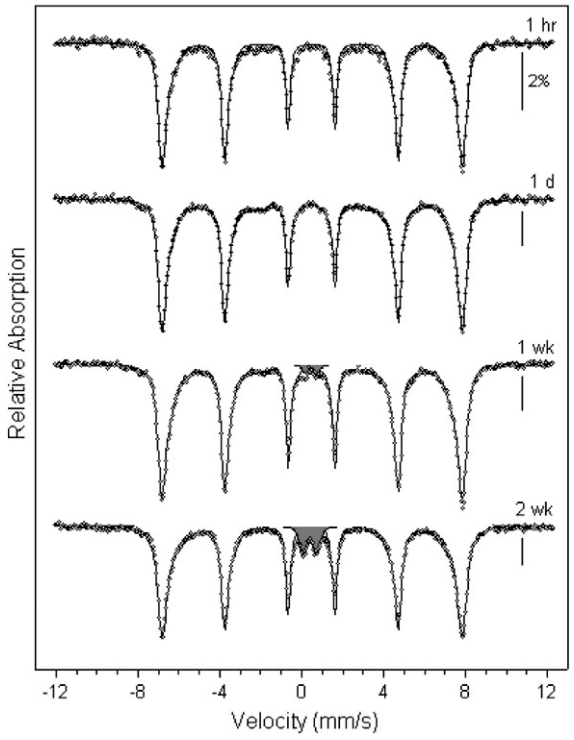

Fig. 3. Mössbauer spectra of lepidocrocite reacted with sulfide after 1 h, 1 day, 1 week, and 2 weeks. White sextets correspond to lepidocrocite, and gray shaded to FeS_2. All spectra were collected at a temperature of 4.2 K. The scale bar represents 2% absorption for each spectrum. Solution conditions are listed in Table 1, and model parameters are listed in Table 3.

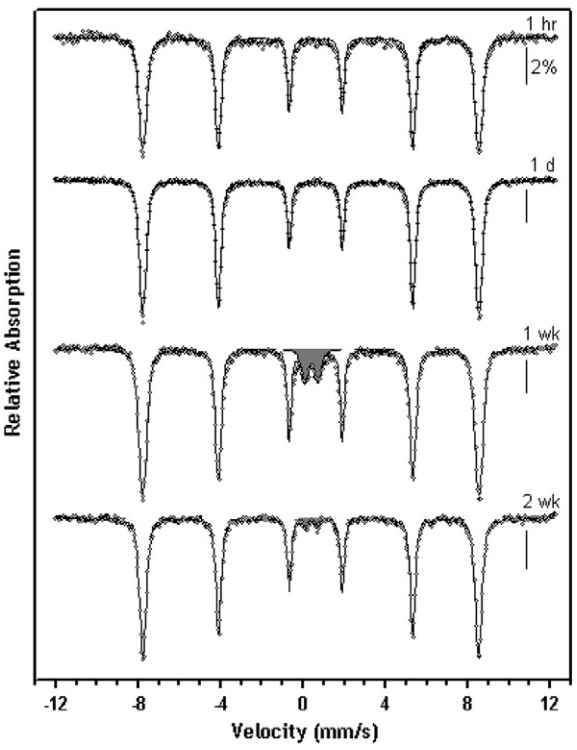

Fig. 4. Mössbauer spectra of goethite reacted with sulfide after 1 h, 1 day, 1 week, and 2 weeks. White sextets correspond to goethite and gray shaded doublets to FeS_2. All spectra were collected at a temperature of 4.2 K. The scale bar represents 2% absorption for each spectrum. Solution conditions are listed in Table 1, and model parameters are listed in Table 3.

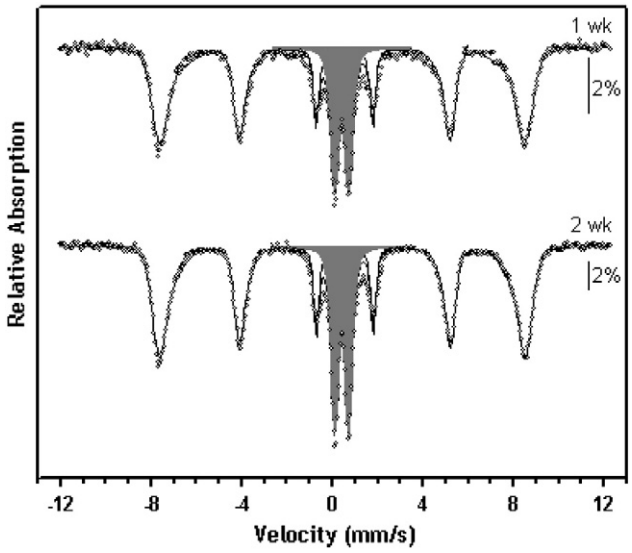

Fig. 5. Mössbauer spectra of ferrihydrite reacted with sulfide after 1 week and 2 weeks. White sextets are bulk models for all Fe(III) (hydr)oxides present and may represent a combination of the goethite, hematite, and magnetite observed by TEM. Gray shaded doublets reflect signals from FeS_2. All spectra were collected at a temperature of 4.2 K. The scale bar represents 2% absorption for each spectrum. Solution conditions are listed in Table 1, and model parameters are listed in Table 3.

end of the second week. In the case of goethite, the signal seems to have decreased with time (Fig. 4). 8.4% of the initially added goethite was transformed into FeS_2 after 1 week with only 2% remaining after 2 weeks (Table 2). This observation, however, needs to be used with caution. Parts of the suspension of the sample taken after 2 weeks seem to have passed the filter during the filtration process so that the recovery of the solid material was probably incomplete in the goethite experiment. Based on these results 26.4%, 6.6%, and at least 2% of the initially added ferrihydrite, lepidocrocite, and goethite, respectively, were converted into FeS_2 after two weeks (Table 2). From these values the concentration of pyrite Fe and consequently that of pyrite S can be derived, which was 6.3 mmol L^{-1} for ferrihydrite, 1.8 mmol L^{-1} for lepidocrocite and 0.9 mmol L^{-1} for goethite. This implies that the conversion efficiency of the initially added S(−II) in this time period varied strongly between the minerals. It was 85% for ferrihydrite, 49% for lepidocrocite and 13% for goethite.

3.2.2. TEM analysis

TEM analyses confirmed the dynamic transformation process occurring upon sulfidation of the various ferric (hydr)oxides. In particular, it revealed insight into the fate of sulfide during the reaction progress which was clearly different between the minerals.

TEM images display well-defined grains of ferrihydrite after 2 h of reaction with dissolved sulfide without any changes in either the morphology of the particles and or their electron diffraction patterns compared to the unreacted starting material. Hence, the almost complete reduction of Fe(III) in the initial phase, as implied by wet chemistry data, has not led to changes in the ferrihydrite structure detectable with TEM. Furthermore, the formation of other distinct different secondary phases was not observed. EDX mapping demonstrated that sulfur was evenly distributed and was probably adsorbed on the ferrihydrite surfaces (Fig. 6d, e) as ferrous polysulfide associations (Wan et al., 2014).

In contrast, the experiments performed with lepidocrocite revealed the formation of sulfur-rich rims around the lepidocrocite crystals that could be attributed to the nucleation of mackinawite by high resolution TEM images and electron diffraction (cf. Fig. 6 in Hellige et al, 2012).

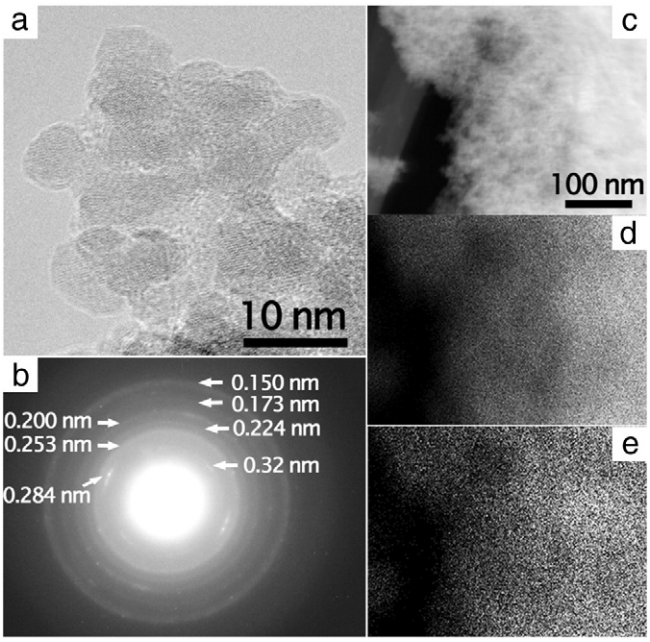

Fig. 6. High resolution TEM image (a) and electron diffraction pattern (b) of ferrihydrite after 2 h reaction with dissolved sulfide. Dark-field STEM image (c) and EDX maps of iron [Fe Kα] (d) and sulfur [S Kα] distribution (e) show that sulfur was evenly distributed on the solid phase.

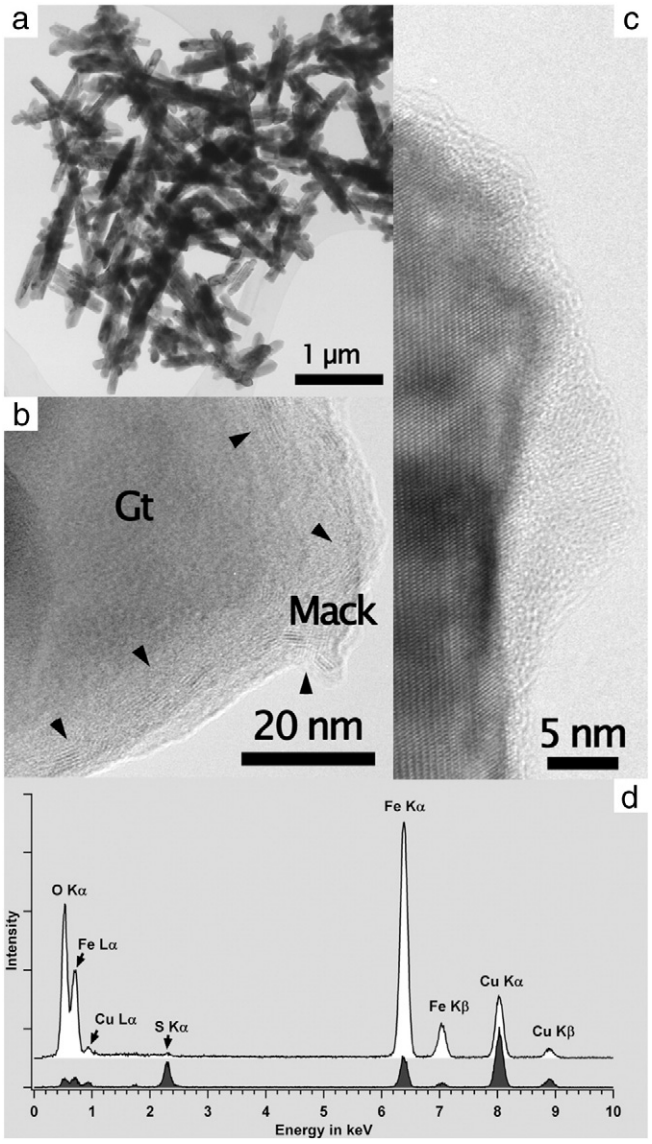

Fig. 7. Bright field TEM image (a) of the apparently pristine particle size and morphology of goethite after 2 h of reaction. High resolution TEM images (b, c) reveal sulfur rich rims on goethite crystals. Lattice fringes in these rims are characteristic for mackinawite (FeS). EDX spectra (d) taken from the rims (black) and in the center of goethite crystals (white) reveal the formation of iron sulfide with a Fe:S ratio close to 1:1 on the goethite surface.

Additionally, a thin layer of magnetite could be identified at the interface between the mackinawite and lepidocrocite structure which disappeared after 2 weeks of reaction (Hellige et al, 2012).

Goethite crystals were surrounded by a layer of mackinawite of variable thickness (Fig. 7b, c) at the end of the first phase of the reaction (2 h). In contrast to lepidocrocite, no evidence for a magnetite layer was found between the goethite core and the surrounding mackinawite layers. Greigite was not detectable in any of the experiments.

After two weeks of reaction, the appearance of particles retrieved from ferrihydrite experiments has changed completely. TEM images confirmed the complete transformation of ferrihydrite and the formation of new phases which is consistent with the chemical data and Mössbauer spectra. Table 4 shows the interplanar spacings (d-values) of the phases which can predominantly be attributed to the structures of magnetite, hematite and pyrite (Fig. 8a, d, e). Only minor amounts of goethite were observed. In contrast to lepidocrocite and goethite, the black coloration of the suspension did not disappear towards the end of reaction which might be due to the very small size (50–100 nm, Fig. 8e) of the newly formed iron oxide particles.

In all samples collected from experiments after two weeks, electron dense particles were detected (Figs. 8a, 9a, cf. also Fig. 8d in Hellige et al., 2012). The morphology of the aggregated assemblages resembles quadric outlines (black squares) indicating an Ostwald ripening process to attain lower surface energy. EDX spectra revealed an Fe:S ratio of 1:2 in the black squares and electron diffraction identified the occurrence of pyrite. All these features point towards the presence of nanocrystalline pyrite domains that may have formed by oriented aggregation (Penn, 2004). These structures were not directly connected to the iron oxide crystals, suggesting that the primary particles formed by precipitation and not solid phase transformation.

Additionally to pyrite, small amounts of hematite were detected in the goethite rims with a thickness of ~20 nm (Fig. 9d), preferably at the top of the acicular goethite crystals.

In conclusion, mineral transformations occurred in experiments with all three oxides during the second phase of the reaction. However, after 2 weeks of reaction the extent of these transformations and the composition of the solids differed. In particular, the formation of other iron oxides and pyrite was less pronounced in experiments with goethite than with lepidocrocite and ferrihydrite, whereas

Table 4
Interplanar spacings and corresponding lattice planes of the phases formed after 14 days of reaction of ferrihydrite with sulfide identified by electron diffraction and fast Fourier transformation of high resolution images.

Pyrite		Hematite		Magnetite		Goethite	
d_{hkl} [Å]	(hkl)	d_{hkl} [Å]	(hkl)	d_{hkl} [Å]	(hkl)	d_{hkl} [Å]	(hkl)
3.12	111	3.70	012	4.86	111	4.18	101
2.71	200	2.76	104	2.95	220	2.72	301
2.42	210	2.54	110	2.52	311	2.56	210
2.21	211	2.23	113	1.48	440	2.24	211/102
1.93	220	1.79	024			2.18	401
1.64	311	1.71	116				
1.47	312	1.46	214/300				
1.21	420						

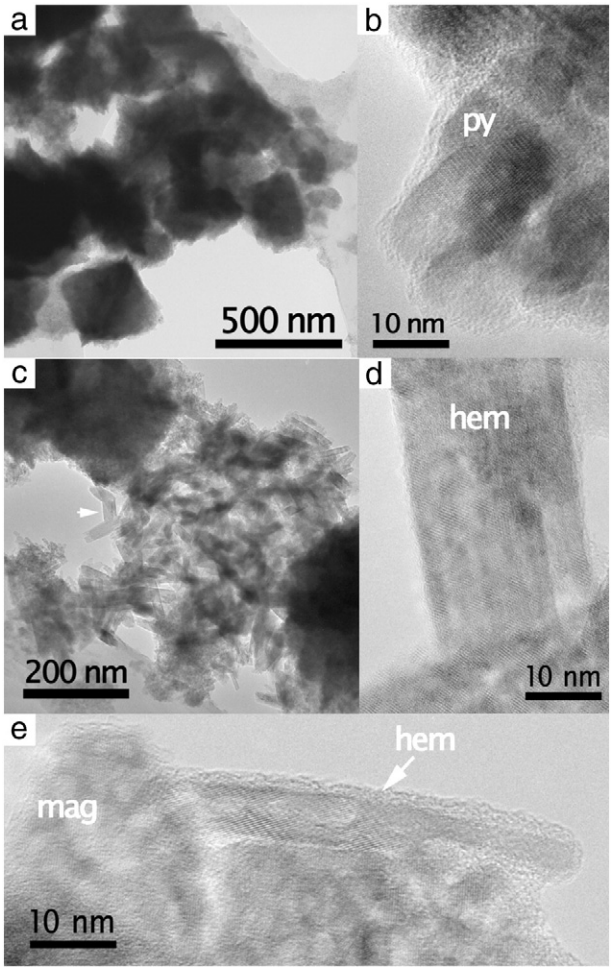

Fig. 8. Bright field (a, c) and high resolution (b, d, e) TEM images after 2 weeks of reaction between ferrihydrite and dissolved sulfide. Pyrite crystals are characterized by quadratic outlines and occur separated from ferric oxides (a, c). The aggregates consisted of agglomerated nanocrystalline domains (b). Ferrihydrite was completely transformed into hematite (arrow in c, d, e) and magnetite (e).

complete transformation into secondary minerals occurred in experiments with ferrihydrite.

4. Discussion

4.1. Formation of excess Fe(II)

Formation of non-sulfur-associated excess Fe(II) is antagonistic to the formation of FeS_s. Mackinawite is a very early product of the interaction between both, lepidocrocite and goethite and dissolved sulfide. A thin layer (~10–20 nm) of mackinawite was observed in the presence of lepidocrocite and goethite. FeS_s turned out to be the largest fraction (50–70%) of surface sulfur species detected with cryostat XPS in a comparable experimental approach (Wan et al., 2014). In contrast, in experiments with ferrihydrite, in which the fraction of excess Fe(II) was highest, no mackinawite was detected. Hence, an inverse relationship seems to exist between the formation of mackinawite and excess Fe(II) within the first hours, which we relate to processes occurring at the mineral surface.

The reductive dissolution of ferric hydroxides is assumed to be preceded by a reversible surface complexation step (Dos Santos Afonso and Stumm, 1992)

$$>Fe_{III}OH + HS^- \leftrightarrow >Fe_{III}S^- + H_2O \quad (2)$$

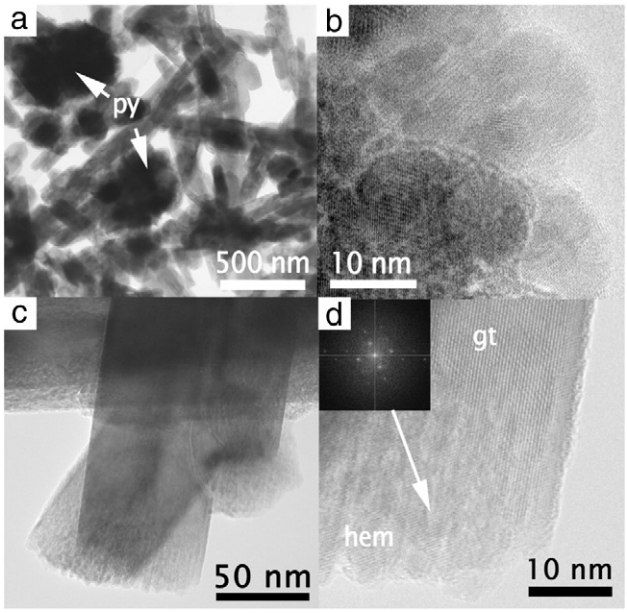

Fig. 9. Bright field TEM image (a) showing the distribution of goethite and pyrite after 2 weeks reaction. The pyrite crystals consisted of nanocrystalline aggregates (b). Bright field TEM images (c, d) and FFT electron diffraction pattern (inset in d) revealed that minor amounts of goethite were transformed into hematite, preferably at the top of the acicular goethite crystals.

which is followed by electron transfer

$$>Fe_{III}S^- \leftrightarrow >Fe_{II}S \quad (3)$$

and the release of an S radical

$$>Fe_{II}S + H_2O \leftrightarrow >Fe_{II}OH_2^+ + S^{\bullet -} \quad (4)$$

that readily reacts further. The rate limiting step is regarded to be the regeneration of a surface site. One possibility for the regeneration of a surface site is the detachment of Fe(II) (Dos Santos Afonso and Stumm, 1992)

$$>Fe_{II}OH_2^+ \rightarrow \text{new surface site} + Fe(II) + H_2O. \quad (5)$$

The consumption rate of dissolved sulfide is different between the three hydroxides. The formation of Fe(II) occurs at a similar rate as the sulfide consumption in all cases (Fig. 1) indicating that the disappearance of dissolved sulfide from solution is not only due to sorption but is directly linked to the electron transfer reaction. Hence, the key to understand the formation of non-sulfur-associated Fe(II) is related to the regeneration mechanism of surface sites (Eq. (5)). At neutral pH, other pathways than release of Fe(II) into solution might be important: electron transfer into the bulk phase and surface precipitation of FeS_s.

Adsorbed Fe(II), which is equivalent to the surface complex $>Fe_{II}OH_2^+$ in Eq. (5), is known to exchange electrons with the bulk phase of various ferric hydroxides. Hiemstra and van Riemsdijk (2007) postulate, based on modeling of charge densities arising from adsorption isotherms, that adsorption of Fe(II) to lepidocrocite requires complete surface oxidation via electron transfer to the bulk mineral,

$$>Fe_{II}OH_2^+ + Fe_{III}(bulk) \xrightarrow{k_{et}} >Fe_{III}OH + Fe_{II}(bulk) + H^+. \quad (6)$$

Goethite and 2-line ferrihydrite revealed a much lower tendency for electron exchange and a larger fraction of adsorbed Fe(II). Pedersen et al. (2005) observed complete electron transfer between adsorbed Fe(II) and bulk $^{55}Fe(III)$ ferrihydrite within 2 days, while goethite and lepidocrocite reacted significantly lower. They measured characteristic

reaction times ($1/k_{obs}$) for electron transfer ranging between 100 min for ferrihydrite and 23,000 min for goethite. Rapid electron transfer was reported by Williams and Scherer (2004) to occur after 6 h equilibration between Fe(II) and bulk goethite and ferrihydrite. Silvester et al. (2005) reported considerable oxidation of Fe(II) upon adsorption onto 2-line ferrihydrite and goethite and its incorporation into the bulk oxide. Jang et al (2008) observed electron transfer between Fe(II) and bulk goethite Fe(III) that reached equilibrium after 7 days with a characteristic reaction time of 1000 min based on measurements of natural abundance isotope fractionation upon adsorption of Fe(II). Interestingly, they could not retrieve the added Fe(II) and attributed this observation to the formation of structurally bound Fe(II), while other researchers were able to recover Fe(II) with dilute HCl from the bulk phase (e.g., Williams and Scherer, 2004). Handler et al (2009), in a similar experimental approach, observed almost complete electron transfer between Fe(II) and bulk goethite within 30 days.

Note, that the electron transfer reported in the literature does not appear to create Mössbauer sensitive Fe(II) entities, which is in line with our observations. Attempts to follow the fate of ^{57}Fe(II) adsorbed onto 2-line ferrihydrite and goethite by Mössbauer spectroscopy failed (Silvester et al, 2005). The authors were not able to detect the Fe(II) character and interpreted this observation as a complete conversion of Fe(II) into the host mineral by electron transfer between adsorbed ^{57}Fe(II) and the surrounding Fe(III) neighbors. Similar observations were made by Williams and Scherer (2004).

As this review shows there is clear evidence from the literature for electron transfer between adsorbed Fe(II) and bulk Fe(III) for all three minerals investigated in this study. It seems, however, that there are distinct differences in the reaction kinetics, with goethite being the slowest reactant and ferrihydrite being the fastest. Electron transfer with ferrihydrite proceeds on the time scale of the initial phase in this study, i.e. the first 2 h.

Alternatively to bulk electron transfer, Fe(II) at the surface may be channeled into FeS_s. The rate of FeS_s formation is very fast with a characteristic reaction time $t_r = 1 / k$ of about ~0.1 s and a dependence on the concentration of total dissolved sulfide (Rickard, 1995). Based on the TEM images it is reasonable to assume growth of mackinawite directly on the host mineral's surface

$$>Fe_{II}OH_2^{+} + HS^- \xrightarrow{k_{FeS}} \text{new surface site} + FeS_{surf} + H_2O. \quad (7)$$

Hence, we can envision two competitive reactions for the regeneration of surface sites: bulk electron transfer that is mineral specific (Eq. (6)) and FeS_s growth that depends on the concentration of dissolved sulfide (Eq. (7)). These considerations explain the different extent of excess Fe(II) formation for the different iron (oxy)hydroxides and also provide a conclusive model for the relationship between the fraction of excess Fe(II) and the initial ratio of dissolved S(−II) concentration to surface-site concentration ($S(-II)_{aq}$:SS ratio) observed in Fig. 10 of Hellige et al (2012). At high ratios reaction (7) is favorable. With decreasing ratios reaction (6) becomes more favorable. The extent of the reaction depends on the specific mineral (Eq. (8)) with k_{et} being the mineral specific pathway controlling parameter (Eq. (8)).

$$\frac{d\{>Fe_{II}OH_2^+\}}{dt} = \begin{cases} -k_{FeS}\cdot\{>Fe_{II}OH_2^+\}\cdot c(HS^-) & \text{high } S(-II)_{aq}\text{:SS ratio} \\ -k_{et}\cdot\{>Fe_{II}OH_2^+\}\cdot c(Fe_{III}(bulk)) & \text{low } S(-II)_{aq}\text{:SS ratio} \end{cases} \quad (8)$$

This model allows us to reinterpret the shape of the fraction of excess Fe(II) data determined in experiments with lepidocrocite plotted as a function of $S(-II)_{aq}$:SS ratios in Fig. 10 of Hellige et al (2012). The inflection point in this Figure reflects the $S(-II)_{aq}$:SS ratio at which the reaction rate for the formation of excess Fe(II) (i.e. electron transfer) exceeds that of FeS_s formation. The rapid electron transfer from Fe(II) to ferrihydrite reported by Pedersen et al (2005) predicts that formation of FeS_s is rather impropable, in agreement with our TEM analyses which do not indicate mackinawite formation. In contrast, the electron transfer rate is low with goethite so that reaction (7) is favorable for this mineral and mackinawite forms at the crystal rims while excess Fe(II) formation is negligible.

4.2. The role of excess Fe(II) as a driver of secondary phase formation

The most striking observation in this study is that the yield of pyrite in relation to the initially added sulfide varies significantly between the three ferric hydroxides and that the fraction of pyrite S after two weeks reaction time is related to formation of excess Fe(II) in the early stage of the reaction (Table 5).

Spontaneous pyrite nucleation from aqueous solution is regarded to occur if a critical oversaturation is exceeded with regard to the activity product $a(Fe^{2+})\ a(H_2S)/a(H^+)^2$ which is reported to be $5.7 \cdot 10^{14}$ at pH 6.5 (Harmandas et al, 1998; Rickard, 2012). It is argued that such a critical value is achieved already if the system is saturated with respect to FeS_s (Rickard, 2012). However, TEM images clearly demonstrate that there is no FeS left at the time when pyrite nanoparticles are precipitating. Further, dissolved sulfide was rapidly consumed to become undetectable ($<10^{-6}$ mol L^{-1} after max 5 h in case of goethite). The maximum oversaturation possible based on this value and a measured dissolved Fe(II) concentration (0.3 mmol L^{-1}) is $2 \cdot 10^{11}$ (no speciation of Fe(II) and no ionic strength considered), which is still three orders of magnitudes lower then the critical value. Hence, nucleation of pyrite from solution species seems improbable.

In our previous paper (Hellige et al, 2012) we have proposed a mechanism which explains the relationship between excess Fe(II) and pyrite formation. According to the mechanism, excess Fe(II) is a reductant for S^0 promoting the formation of pyrite through generation of polysulfides, which are regarded key precursors for the formation of pyrite (e.g., Rickard and Luther, 2007)

$$2\,Fe^{2+}_{excess} + S_n + 4H_2O \leftrightarrow 2FeOOH + S_n^{2-} + 6H^+. \quad (9)$$

Interestingly, no or only small amounts of dissolved polysulfides could be detected in comparable experiments while a substantial fraction of surface bound sulfur consisted of polysulfides (Wan et al., 2014). We therefore propose that dissolved polysulfides may react with surface bound Fe(II) to form surface bound precursors of pyrite.

HCl extractable Fe(II) as well as MES were significantly reduced or even disappeared in experiments with the three different iron oxyhydroxides after 14 days supporting the model proposed in reaction (9). Based on the stoichiometry of reaction (9), protons are generated which can explain the drop in pH in experiments with lepidocrocite and ferrihydrite (Fig. 2). Formation of surface-bound polysulfides gives rise to pyrite precipitation as suggested by the appearance of pyrite in Figs. 8a and 9a of this paper and Fig. 8d in Hellige et al (2012), implying that pyrite is not formed by solid phase transformation.

Besides the formation of pyrite, the unidentified fraction of excess Fe(II) might also trigger the transformation of ferrihydrite and

Table 5
Relationship between fraction of excess Fe(II) after 2 h (lepidocrocite and ferrihydrite) or 8 h (goethite) reaction time and pyrite yield after 14 days.

	Ferrihydrite	Lepidocrocite	Goethite
Fraction of excess Fe(II) after 2–8 h [% of $Fe(II)_{HCl}$]	46	36	0
Fraction of pyrite S after 14 days [% of initial S(−II)]	84	50	13

lepidocrocite into iron (hydr)oxides with higher thermodynamic stability. Electron transfer between adsorbed Fe^{2+} and the bulk mineral is known to stimulate transformation of the receiving mineral (Cornell and Schwertmann, 2003). Indeed, secondary formation of iron oxyhydroxides occurred in experiments with all three initial materials but at different rates and at different extent. The most pronounced alterations happened with ferrihydrite. Selected area electron diffraction indicates that the ferrihydrite structure remained intact after 2 h of reaction (Fig. 6). After one week, ferrihydrite transformed into a mixture of hematite, goethite and magnetite. Consumption of HCl was much lower compared to the other oxides (Fig. 2) which is a clear hint to the generation of protons along with the formation of the transformation products taking place already in a very early stage, e.g., during the formation of magnetite (for simplicity reasons we have used the stoichiometric formula $Fe(OH)_3$ for ferrihydrite in Eq. (10)):

$$2Fe(OH)_3 + Fe^{2+} \rightarrow Fe_3O_4 + 2H_2O + 2H^+. \quad (10)$$

Ferrihydrite has a similar anionic framework as hematite with the same stacking of close-packed anions. Liu et al. (2009) proposed that the nucleation and growth of hematite from ferrihydrite involved a combination of dehydration and rearrangement processes which are facilitated by the structural resemblance between these two minerals.

In contrast, goethite and magnetite are products related to Fe(II) driven transformation (Cornell and Schwertmann, 2003). Pedersen et al. (2005) observed complete ferrihydrite transformation into goethite at an aqueous Fe(II) concentration of 1 mmol L^{-1} within 2 days. They found, however, that lepidocrocite is the main product at a lower Fe(II) concentration of 0.2 mmol L^{-1}. Similarly, the occurrence of magnetite also seems to depend on aqueous Fe(II) concentration, with magnetite being generated from ferrihydrite at high concentrations (~2 mmol L^{-1}) only (Hansel et al, 2005). Pedersen et al (2005) observed magnetite as a product from transformation of lepidocrocite at their highest experimental aqueous Fe(II) concentration of 1 mmol L^{-1}.

High concentrations of ferrous iron in solution also reflect a high degree of adsorbed Fe(II). Hence, the occurrence of goethite and magnetite as transformation products may also be related to the amount of excess Fe(II) so that this entity may drive transformation pathways in our systems. For example, magnetite forms as an intermediate layer between the lepidocrocite crystal and mackinawite surface coverage after reaction with sulfide (Hellige et al, 2012), while no magnetite is observed in experiments with goethite when no excess Fe(II) is produced.

Surprisingly, no transformation after reaction with aqueous Fe(II) has been reported for goethite although significant isotopic exchange between aqueous Fe(II) and solid phase Fe(III) could be observed (Pedersen et al., 2005; Jang et al., 2008; Handler et al., 2009). Handler et al (2009) interpreted this effect in terms of conveyer-belt model according to which electron transfer occurs, but the new Fe(III) will lead to isostructural growth at separate goethite surface sites with now reduced Fe(II) being released back into solution. It remains speculative as to whether such a response to Fe(II) adsorption would also explain the reaction kinetics between sulfide and the goethite surface and thus the low formation rate of excess Fe(II). However, it becomes clear that no reductive transformation product should be expected in the goethite experiments. The traces of hematite observed at the top of acicular goethite crystals are probably due to a ripening process.

5. Conclusion

The results of this work give reason to the proposition of pathway for rapid pyrite formation that is based on three steps: i) sulfidation of ferric hydroxides, ii) generation of bulk electrons, and iii) generation of (surface bound) polysulfides by bulk electrons. These reactions are accompanied by a series of transformation steps. Depending on the iron hydroxide phase and the initial concentration of dissolved S(−II), different pathways of solid product formation appear on both, the ferric hydroxide side and the sulfur side, which implies a clear kinetic control of these reactions that are of high relevance for early diagenetic processes.

We propose that it is the rate of surface polysulfide generation (Eq. (9)) and subsequent reaction with precursors bound to the host mineral's surface that controls the overall rate of this sulfidation pathway. Pyrite formation pathways based on dissolution of solid FeS_n to aqueous FeS (FeS-pathway) and subsequent reactions with dissolved polysulfides in the absence of ferric oxides are comparatively slow (on the order of several months to years, e.g., Luther, 1991). Hence, the sulfidation pathway needs to be considered in environments that operate on the time scale of days and weeks and that are subject to redox oscillations, such as tidal flats, wetlands, riparian soils, the sediment–water interface, or the capillary fringe in ground water systems. Ferrihydrite and lepidocrocite are characteristic for such environments with rapid redox recycling of Fe(II) (Cornell and Schwertmann, 2003). They present a high potential for excess Fe(II) formation and are therefore candidates to stimulate rapid formation of pyrite and transformation of the host ferric mineral in such environments. In contrast, the occurrence of goethite typically reflects matured environments that allowed for sufficient ripening time, although goethite specimen of high reactivity are also existing (e.g., van der Zee et al, 2003).

We have demonstrated that dissolved sulfide interacts with ferric hydroxides in two ways. It generates Fe(II) (respectively excess electrons) driving transformations of these minerals and it is a sulfide source for FeS_s formation. The extent of FeS_s and/or Fe(II) formation, however, seems to depend on the ratio between dissolved sulfide and the amount of surface sites (SS) available (Hellige et al, 2012).

At low $S(-II)_{aq}$:SS ratios, the concentration of dissolved sulfide is low relative to the concentration of reactive surface sites, which matches conditions in environments that are often abundant in ferric hydroxides and in which sulfide may be continually supplied e.g., through microbial reduction or diffusion. From these considerations a geochemical window can be derived that supports the occurrence of the sulfidation pathway (Fig. 10).

Rapid pyrite formation (on a time scale of days) has been observed in such environments (Howarth, 1979; Otero and Macias, 2002). Pyrite formation was attributed to direct precipitation of pyrite with Fe^{2+} and polysulfides (Giblin and Howarth, 1984; Giblin, 1988), the polysulfides being assumed to be products of a not specified oxidation of sulfide. Similar to our experiments (except the first couple of hours), concentrations of dissolved sulfide were low (1–20 μmol L^{-1}) probably due to consumption by ferric iron. Polysulfides were not measured in these studies. In a study on reflooding a formerly drained coastal wetland, Burton et al (2011) observed decoupling of pyrite and AVS/greigite formation and could not relate its formation to the classical pathway via mackinawite. In the light of our study pyrite formation in such systems occurred under conditions where dissolved sulfide is produced but maintained at low concentrations by high amounts of reactive ferric (hydr)oxides and therefore allows for a high fraction of excess Fe(II).

In contrast, high $S(-II)_{aq}$:SS ratios reflect conditions in marine systems (or specific sulfate-rich terrestrial environments) with a high supply of organic material to stimulate sulfate reduction. According to the results derived in the present work, the formation of excess Fe(II) and its rapid conversion into pyrite would be suppressed by the fast formation of FeS_s if the reactivity of the iron minerals towards sulfide is low (e.g., Canfield et al., 1992). Such conditions exist where the reoxidation of Fe(II) to generate low crystallinity Fe(III) phases is impeded and the iron mineralogy is controlled by deposition of specimen of higher crystallinity, such as goethite (and probably also hematite although we did not study this mineral). We propose that the anomalous accumulation of acid volatile sulfide at 40 cm depth of a fjord in the presence of low dissolved sulfide concentrations reflects such conditions (Gagnon et al, 1995). Similar observations were made at the sulfidation front at a depth of ~300 cm depth in a Black Sea sediment (Jørgensen et al, 2004), where AVS accumulated upon reaction of sulfide with reactive

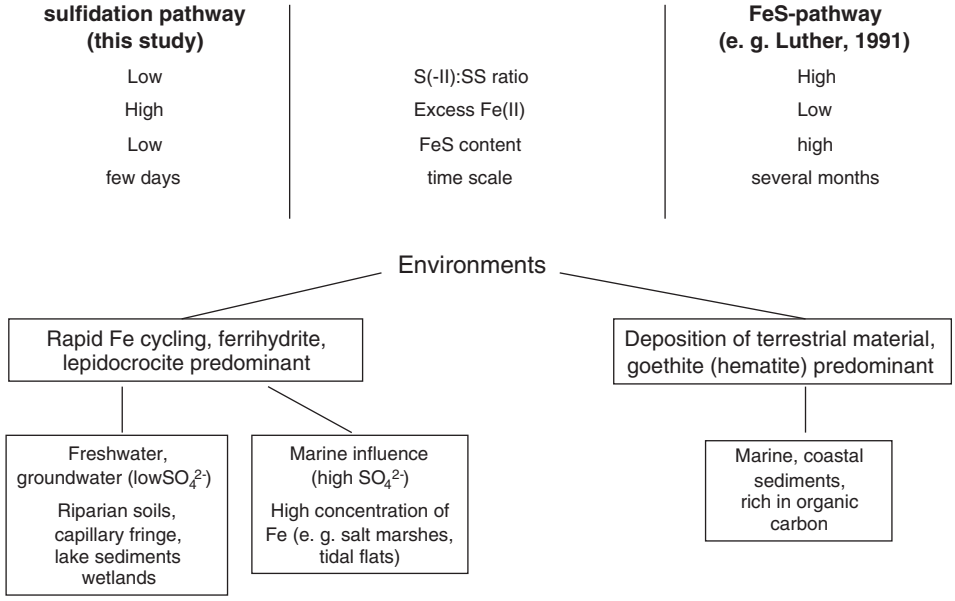

Fig. 10. Scheme for the classification of environments according to their potential for rapid pyrite formation.

iron. It is reasonable to assume that "reactive iron" at this depth is not a high surface-area material so that reaction pathway (7) may be faster than electron transfer to the bulk mineral (reaction (6)) under these conditions.

This short discussion cannot encompass and revisit the entire body of pyrite formation studies but it underpins that the specific reactivity of iron minerals towards sulfide needs to be considered when discussing the formation of pyrite and of other secondary minerals.

Our study has emphasized the role of an adsorption step preceding the entire sulfidation mechanism. It has been demonstrated that the reactivity of iron minerals can be significantly affected by interfering adsorbates. Phosphate even inhibited reductive dissolution of ferric (hydr)oxides (Biber et al., 1994). Hence, the role of important constituents of natural waters such as DOC or Si in affecting the sulfidation reaction needs to be tested in order to refine our understanding of the response of natural systems rich in these compounds on the interaction between ferric (hydr)oxides and dissolved sulfide.

An interesting novel observation is the decoupling of reaction times during the interaction between sulfide and ferric hydroxides. Generation of excess Fe(II), which we identified as a requirement for pyrite formation, occurs within hours, while the formation of pyrite takes place within days. This phenomenon may be regarded as a process of charging the ferric minerals with electrons prior to consumption along with the pyrite formation process. Under conditions, where redox fluctuations occur on a time scale shorter than that of the formation of pyrite (e.g., tidal fluctuations), excess Fe(II) may thus exert some reactivity towards other oxidants than elemental sulfur (e.g., humic acids) and transfer electrons. Conceptually, electron transfer from sulfide to the bulk ferric mineral may thus be regarded as the build-up of electric capacity in a dynamic redox system, the role of which for other electron transfer processes being far from understood.

Acknowledgments

This research was funded by the Deutsche Forschungsgemeinschaft (DFG) and part of the priority program 580 "Electron Transfer Processes in Anoxic Aquifers" (PE 438/11-2). Kilian Pollok was supported by grant 03G0718A from the R&D programme Geotechnologien. We thank Stefan Haderlein and Andreas Kappler, University of Tübingen for using their Mössbauer spectroscopic instrument. Christian Schröder is acknowledged for the fruitful discussions. We also thank the staff members of the Department of Hydrology, University of Bayreuth for help and support.

References

Biber, M.V., Dos Santos Afonso, M., Stumm, W., 1994. The coordination chemistry of weathering: IV. Inhibition of the dissolution of oxide minerals. Geochim. Cosmochim. Acta 59, 1999–2010.
Bonneville, S., Behrends, T., Van Cappellen, P., 2009. Solubility and dissimilatory reduction kinetics of iron(III) oxyhydroxides, a linear free energy relationship. Geochim. Cosmochim. Acta 73 (18), 5273–5282.
Burton, E.D., Bush, R.T., Johnston, S.G., Sullivan, L.A., Keene, A.F., 2011. Sulfur biogeochemical cycling and novel Fe–S mineralization pathways in a tidally re-flooded wetland. Geochim. Cosmochim. Acta 75, 3434–3451.
Canfield, D.E., Raiswell, R., Bottrell, S., 1992. The reactivity of sedimentary iron minerals toward sulphide. Am. J. Sci. 292, 659–683.
Cornell, R.M., Schwertmann, U., 2003. The Iron Oxides. Wiley-VCH (664 pp.).
Dos Santos Afonso, M., Stumm, W., 1992. Reductive dissolution of iron(III) (hydr)oxides by hydrogen sulphide. Langmuir 8, 1671–1675.
Einsele, W., 1936. Über die Beziehungen des Eisenkreislaufes zum Phosphatkreislauf im Eutrophen See. Arch. Hydrobiol. 29, 664–686.
Ferdelman, T.G., Church, T.M., Luther, G.W., 1991. Sulfur enrichment of humic substances in a Delaware salt marsh sediment core. Geochim. Cosmochim. Acta 55, 979–988.
Fischer, W.R., 1987. Standard potentials (Eo) of iron(III) oxides under reducing conditions. Z. Pflanzenernähr. Bodenkd. 150, 286–289.
Fonselius, S., Dyrssen, D., Yhlen, B., 1999. Determination of hydrogen sulphide. In: Grasshoff, K., Kremling, K., Ehrhardt, M. (Eds.), Methods of Seawater Analysis. Wiley-VCH, Weinheim, New York, Chichester, Brisbane, Singapore, Toronto, pp. 91–108.
Gagnon, C., Mucci, A., Pelletier, E., 1995. Anomalous accumulation of acid-volatile sulfides in a coastal marine sediment, Saguenay Fjord, Canada. Geochim. Cosmochim. Acta 59, 2663–2676.
Giblin, A.E., 1988. Pyrite formation in marshes during early diagenesis. Geomicrobiol. J. 6, 77–97.
Giblin, A.E., Howarth, R.W., 1984. Porewater evidence for a dynamic sedimentary iron cycle in salt marshes. Limnol. Oceanogr. 29, 47–65.
Gorski, C.A., Scherer, M.M., 2009. Influence of magnetite stoichiometry on FeII uptake and nitrobenzene reduction. Environ. Sci. Technol. 43, 3675–3680.
Gorski, C.A., Scherer, M.M., 2012. Fe^{2+} sorption at the Fe oxide–water interface: a revised conceptual framework. In: Tratnyek, P.G., Grundl, T.J., Haderlein, S.B. (Eds.), Aquatic Redox Chemistry. ACS Symp. Ser. 1071, pp. 315–343 (Chapter 15).
Haderlein, S.B., Pecher, K., 1998. Pollutant reduction in heterogeneous Fe(II)/Fe(III)-systems. In: Sparks, D.L., Grundl, T. (Eds.), Kinetics and Mechanisms of Reactions at the Mineral/Water Interface. ACS Symp. Ser. 715, pp. 342–357 (Chapter 17).
Handler, R.M., Beard, B.L., Johnson, C.M., Scherer, M.M., 2009. Atom exchange between aqueous Fe(II) and goethite: an Fe isotope tracer study. Environ. Sci. Technol. 43, 1102–1107.
Hansel, C.M., Benner, S.G., Fendorf, S., 2005. Competing Fe(II)-induced mineralization pathways of ferrihydrite. Environ. Sci. Technol. 39, 7147–7153.
Harmandas, N.G., Navarro-Fernandez, E., Koutsoukos, P.G., 1998. Crystal growth of pyrite in aqueous solutions. Inhibition by organophosphorus compounds. Langmuir 14, 1250–1255.

Hellige, K., 2011. The Reactivity of Ferric (Hydr)oxides Towards Dissolved Sulphide. Dissertation Thesis. Fakultät für Biologie, Chemie und Geowissenschaften. Universität Bayreuth.
Hellige, K., Pollok, K., Larese-Casanova, P., Behrends, T., Peiffer, S., 2012. Pathways of ferrous iron mineral formation upon sulfidation of lepidocrocite surfaces. Geochim. Cosmochim. Acta 81, 69–81.
Hiemstra, T., van Riemsdijk, W.H., 2007. Adsorption and surface oxidation of Fe(II) on metal (hydr)oxides. Geochim. Cosmochim. Acta 71 (24), 5913–5933.
Howarth, R.W., 1979. Pyrite: its rapid formation in a salt marsh and its importance in ecosystem metabolism. Science 203, 49–51.
Jang, J.H., Mathur, R., Liermann, L.J., Ruebush, S., Brantley, S.L., 2008. An iron isotope signature related to electron transfer between aqueous ferrous iron and goethite. Chem. Geol. 250 (1–4), 40–48.
Jørgensen, B.B., Böttcher, M.E., Lüschen, H., Neretin, L.N., Volkov, I.I., 2004. Anaerobic methane oxidation and a deep H_2S sink generate isotopically heavy sulfides in Black Sea sediments. Geochim. Cosmochim. Acta 68, 2095–2118.
Larese-Casanova, P., Scherer, M.M., 2007. Fe(II) sorption on hematite: new insights based on spectroscopic measurements. Environ. Sci. Technol. 41, 471–477.
Liu, H., Guo, H., Li, P., Wei, Y., 2009. Transformation from δ-FeOOH to hematite in the presence of trace Fe(II). J. Phys. Chem. Solids 70, 186–191.
Luther, I.G.W., 1991. Pyrite synthesis via polysulfide compounds. Geochim. Cosmochim. Acta 55, 2839–2849.
Murad, Cashion, 2004. Mössbauer Spectroscopy of Environmental Materials and Their Industrial Utilization. Kluwer Academic Publishers.
Otero, X.L., Macias, F., 2002. Variation with depth and season in metal sulfides in salt marsh soils. Biogeochemistry 61, 247–268.
Pedersen, H.D., Postma, D., Jakobsen, R., Larsen, O., 2005. Fast transformation of iron oxyhydroxides by the catalytic action of aqueous Fe(II). Geochim. Cosmochim. Acta 69, 3967–3977.
Peiffer, S., Gade, W., 2007. Reactivity of ferric oxides toward H_2S at low pH Environ. Sci. Technol. 41, 3159–3164.
Peiffer, S., Dos Santos Afonso, M., Wehrli, B., Gächter, R., 1992. Kinetics and mechanism of the reaction of H_2S with lepidocrocite. Environ. Sci. Technol. 26 (12), 2408–2413.
Penn, R.L., 2004. Kinetics of oriented aggregation. J. Phys. Chem. 108, 12707–12712.
Postma, D., 1993. The reactivity of iron oxides in sediments — a kinetic approach. Geochim. Cosmochim. Acta 57, 5027–5034.
Poulton, S.W., Krom, D.M., Raiswell, R., 2004. A revised scheme for the reactivity of iron (oxyhydr)oxide minerals towards dissolved sulfide. Geochim. Cosmochim. Acta 68 (18), 3703–3715.
Pyzik, A.J., Sommer, S.E., 1981. Sedimentary iron monosulphides: kinetics and mechanism of formation. Geochim. Cosmochim. Acta 45, 687–698.
Raiswell, R., Canfield, D.E., 2011. The iron biogeochemical cycle past and present. Geochem. Perspect. 1, 1–220.
Rickard, D., 1974. Kinetics and mechanism of the sulfidation of goethite. Am. J. Sci. 274, 941–952.
Rickard, D., 1975. Kinetics and mechanism of pyrite formation at low temperatures. Am. J. Sci. 275, 636–652.
Rickard, D., 1995. Kinetics of FeS precipitation: part 1. Competing reaction mechanisms. Geochim. Cosmochim. Acta 59 (21), 4367–4380.
Rickard, D., 2012. Sulfidic sediments and sedimentary rocks. Developments in Sedimentology 65. Elsevier (801 pp.).
Rickard, D., Luther, G.W., 2007. Chemistry of iron sulphides. Chem. Rev. 107 (2), 514–562.
Roden, E.E., 2003. Fe(III) oxide reactivity toward biological versus chemical reduction. Environ. Sci. Technol. 37, 1319–1324.
Schwertmann, U., Cornell, R.M., 2000. Iron Oxides in the Laboratory: Preparation and Characterization. Wiley-VCH Verlag GmbH, Weinheim, New York, Basel, Cambridge, Tokyo (188 pp.).
Silvester, E., et al., 2005. Redox potential measurements and Mossbauer spectrometry of Fe-II adsorbed onto Fe-III (oxyhydr)oxides. Geochim. Cosmochim. Acta 69, 4801–4815.
Tamura, H., Goto, K., Yotsuyanagai, T., M., N., 1974. Spectrophotometric determination of iron(II) with 1,10-phenanthroline in the presence of large amounts of iron(III). Talanta 21, 314–318.
Thamdrup, B., 2000. Bacterial manganese and iron reduction in aquatic sediments. In: Schink, B. (Ed.), Advances in Microbial Ecology vol. 16. Kluwer Academic, New York, pp. 41–83 (chapt. 2).
van der Zee, C., Roberts, D.R., Rancourt, D.G., Slomp, C.P., 2003. Nanogoethite is the dominant reactive oxyhydroxide phase in lake and marine sediments. Geology 31, 993–996.
Wan, M., Shchukarev, A., Lohmayer, R., Planer-Friedrich, B., Peiffer, S., 2014. The occurrence of surface polysulphides during the interaction between ferric (hydr)oxides and aqueous sulphide. Environ. Sci. Technol. 48, 5076–5084.
Williams, A.G.B., Scherer, M.M., 2004. Spectroscopic evidence for Fe(II)–Fe(III) electron transfer at the iron oxide–water interface. Environ. Sci. Technol. 38, 4782–4790.